Chinese Journal of
POLYMER SCIENCE

RESEARCH ARTICLE

https://doi.org/10.1007/s10118-023-3051-y
Chinese J. Polym. Sci. **2024**, *42*, 311–321

Random Terpolymer Based on Simple Siloxane-functionalized Thiophene Unit Enabling High-performance Non-fullerene Organic Solar Cells

Fuliang Cheng[a], Shiting Lai[a], Yihan Zhang[a], Ling Xue[a], Xinxin Xia[b], Peipei Zhu[a], Xinhui Lu[b], Xunfan Liao[a*], and Yiwang Chen[a,c*]

[a] *National Engineering Research Center for Carbohydrate Synthesis/Key Laboratory of Fluorine and Silicon for Energy Materials and Chemistry of Ministry of Education, College of Chemistry and Chemical Engineering, Jiangxi Normal University, Nanchang 330022, China*
[b] *Department of Physics, Chinese University of Hong Kong New Territories, Hong Kong 999077, China*
[c] *Institute of Polymers and Energy Chemistry (IPEC)/Jiangxi Provincial Key Laboratory of New Energy Chemistry, Nanchang University, Nanchang 330031, China*

Electronic Supplementary Information

Abstract Incorporation of siloxane-functionalized units into polymers backbone has proven to be an efficient strategy to improve photovoltaic performance. In this work, a low-cost siloxane-containing unit was developed to construct a series of terpolymers, and the effects of siloxane on the polymer performance were systematically studied. Different contents of thiophene containing siloxane-functionalized side chain were introduced into PM6 to obtain a series of polymers (PM6, PM6-SiO-10, PM6-SiO-20 and PM6-SiO-30). The siloxane-functionalized side chains in polymers have only a slight effect on the absorption behavior and frontier molecular orbitals. However, when the siloxane content increased, the terpolymers' aggregation property decreased and the temperature-dependency increased, leading to improved donor-acceptor compatibility. The power conversion efficiency (PCE) based on PM6:Y6, PM6-SiO-20:Y6 and PM6-SiO-30:Y6 devices was 15.64%, 16.03% and 15.82%, respectively. In comparison, the active layer based on PM6-SiO-10:Y6 exhibits the most appropriate phase separation morphology, resulting in effective exciton dissociation, more balanced hole-electron transport and less recombination. Consequently, the highest PCE of 16.69% with an outstanding short-circuit current density of 26.96 mA·cm^{-2} was obtained, which are one of the highest values for siloxane-functionalized polymer-based devices. This work demonstrates that finely controlling the content of siloxane-functionalized thiophene is beneficial for obtaining high-performance terpolymer donors and provides a novel and low-cost method to improve photovoltaic performance.

Keywords Organic solar cells; Terpolymers; Siloxane-functionalized unit; Low-cost; Morphology

Citation: Cheng, F.; Lai, S.; Zhang, Y.; Xue, L.; Xia, X.; Zhu, P.; Lu, X.; Liao, X.; Chen, Y. Random terpolymer based on simple siloxane-functionalized thiophene unit enabling high-performance non-fullerene organic solar cells. *Chinese J. Polym. Sci.* **2024**, *42*, 311–321.

INTRODUCTION

Due to the lightweight, low cost, ability to be processed through solution methods, and suitability for flexible roll-to-roll production, organic solar cells (OSCs) are considered as a promising next-generation photovoltaic technology.[1–7] In the past decade, great efforts have been devoted into the development of narrow bandgap (E_g<1.6 eV) non-fullerene acceptors (NFAs),[8–11] wide bandgap (WBG) polymer donors,[12,13] active layer morphological optimization techniques,[14–16] and device structure optimization techniques.[17–19] Currently, the power conversion efficiency (PCE) of the cutting-edge single-junction OSCs has succeeded over 19%.[16,19] In particular, the rapid development of narrow bandgap NFAs represented by Y-series greatly boosted the PCE of OSCs due to their strong absorption in the long wavelength range, low energy loss and excellent three-dimensional network stacking.[8,20,21] In order to fully utilize sunlight, the develop of WBG polymer donors with complementary absorption and excellent morphology is an urgently need, and which are of great importance for further improving the device short-circuit current density (J_{SC}) and PCE.[22–24]

PM6 is currently one of the best performing and most universal polymer donor, which has attracted great attentions due to its appropriate energy level, strong crystallinity and a face-on dominated molecular orientation.[16,25,26] In order to match the high performance and a wider range of NFAs, the high-performance polymer donor material library needs to be filled. To achieve high-performance OSCs, several approaches were employed in the development of novel donor-acceptor (D-A) alternating copolymers: (a) the construction of high-performance electron-donating (D) units and electron-ac-

* Corresponding authors, E-mail: xfliao@jxnu.edu.cn (X.L.)
E-mail: ywchen@ncu.edu.cn (Y.C.)

Received July 20, 2023; Accepted September 8, 2023; Published online November 2, 2023

cepting (A) units;[27–29] (b) optimizing side chain (alkyl, alkoxy, alkylthio, and carboxylate) to achieve appropriate crystallinity and form nanoscale interpenetrating networks;[30–32] (c) introducing halogen atoms (F, Cl) to adjust the photoelectric properties.[33–35] Although these strategies have been highly successful, the structural optimization involved unavoidably introduces complexities to the synthetic pathway, leading to unpredictable yields and increased costs. In contrast to extensive structural modifications, the introduction of a third unit within the polymer backbone through terpolymerization has emerged as an effective and cost-efficient strategy. For example, Zhang *et al*. used simple units, such as 3,6-dithiophenyl-2-carboxylate pyrazine (DTCPz),[36] thiophene[37] and thiophene-thiazolothiazole (TTz)[38] as the third unit to obtain terpolymers with excellent properties. However, in order to obtain the terpolymerization strategy with appropriate nanoscale interpenetrating networks and excellent active layer morphology, it is important to develop an effective and cost-effective third unit.

The siloxane-functionalized side chain is a unique solubilizing side chain, which supplies a branch point far from the conjugated main chain and the bulky with steric hindrance effect to provide sufficient solubility for the polymer. Bao *et al*. utilized the particularity of the siloxane-functionalized side chains to decrease the π-π stacking distance of isoindigo-based polymer, thereby improved the lateral mobility.[39] In contrast, the incorporation of siloxane-functionalized side chains enhances the face-on stacking orientation of the polymer, thereby promoting high charge mobility. This effect is exemplified by the improved photovoltaic performance observed when alkyl chains are replaced with siloxane-functionalized side chains in PTB7-Th.[40] Finally, the content of the siloxane-functionalized side chain also has a great influence on the energy level, solubility, crystallinity and crystal orientation of the polymer.[41–43] The modification effect of siloxane-functionalized side chains is very significant, but the cost of siloxanation synthesis of common groups such as benzodithiophene (BDT),[43] benzotriazole (BTA),[43–45] pyrrolo[3,4-*f*]benzotriazole-5,7-dione (TzBI),[44,45] diketopyrrole[46] is high, which is not conducive to the popularization of siloxane.

In this work, different contents (0%, 10%, 20% and 30%) of thiophene with siloxane-functionalized side chain were introduced into the PM6 skeleton to obtain a series of polymers (PM6, PM6-SiO-10, PM6-SiO-20 and PM6-SiO-30). Thiophene as siloxane-functionalized side chain connection unit, which not only reduces the cost of siloxanization synthesis, but also makes full use of the branch point of the siloxane-functionalized side chain away from the conjugated main chain and the bulky with steric hindrance effect to adjust the crystallinity of the terpolymers. Grazing incidence wide angle X-ray scattering (GIWAXS) results indicated that when 10% thiophene with siloxane-functionalized side chain units incorporated into PM6, the crystal coherence length (CCL) of (010) out-of-plane (OOP) peak significantly decreased, which mainly due to the introduction of the third unit by terpolymerization destroying the original ordered molecular arrangement. However, the CCL of the π-π stacking increased as the content of siloxane-functionalized thiophene units further increased, indicating that siloxane can inhibit the disorder in molecular arrangement due to random copolymerization. On the other hand, the side chain density decreases with the increase of the content of siloxane-functionalized thiophene, which affects the crystallinity and the nanoscale interpenetration network of the polymer chain. When Y6 was employed as the acceptor, PM6-SiO-10 based device obtained the highest PCE of 16.69% with an open-circuit voltage (V_{OC}) of 0.850 V, a J_{SC} of 26.96 mA·cm^{-2}, and an FF of 72.84%. While the PM6, PM6-SiO-20 and PM6-SiO-30-based devices showed PCEs of 15.64%, 16.03%, and 15.82%, respectively. Our work demonstrates that the introduction of an appropriate unit of siloxane-functionalized unit is effective and feasible in constructing high-performance polymers for OSCs.

EXPERIMENTAL

Materials

6-Bromo-1-hexene, Mg, I_2, NBS, Ni(dppp)$_2$Cl$_2$, chloroform, PEDOT:PSS, Ag (99.999%) were purchased from Beijing Innochem Technology Co., Ltd., and used without further purification.

Synthesis of Compound 4 and Polymers

A detailed synthesis route of thiophene with siloxane-functionalized side chain (compound 4) is shown in Fig. 1(a) and in the electronic supplementary information (ESI, Fig. S1). Compound 4 was obtained from 6-bromohexyl-1-ene in four steps. 6-Bromohexyl-1-ene was first prepared by Mg and iodine to form Grignard reagent compound 1. Second, compound 1 was added to a solution containing 3-bromothiophene and Ni(dppp)$_2$Cl$_2$ to obtain compound 2. Then, compound 2 was dissolved in toluene, and 1,1,1,3,5,5,5-heptamethyltrisiloxane and Kamstedt catalyst were gradually added dropwise to the solution, resulting in the product of compound 3. Finally, compound 3 was brominated with *N*-bromosuccinimide (NBS) to obtain compound 4. The ^{1}H-NMR characterization of the corresponding compounds can be found in Figs. S2–S4 (in ESI). The polymers PM6, PM6-SiO-10, PM6-SiO-20 and PM6-SiO-30 were prepared *via* Stille copolymerization using Pd(PPh$_3$)$_4$ as the catalyst and adding compound 4, BDD-Br and BDT-Sn unit with different molar ratios (Fig. 1b). The crude polymers were sequentially extracted and purified with methanol, acetone, hexane and dichloromethane until the extract solvent was colorless. Finally, the chloroform solution was concentrated and precipitated in methanol, filtered precipitate and vacuum dried to obtain the targeted polymers. The molecular weight of the polymers was determined by high-temperature gel permeation chromatography (HT-GPC) at 150 °C using 1,2,4-trichlorobenzene as the eluent. The number-average molecular weights (M_n) of PM6, PM6-SiO-10, PM6-SiO-20 and PM6-SiO-30 were 35.35, 30.51, 35.95 and 34.94 kDa with a corresponding polydispersity index (PDI) of 2.04, 2.23, 2.18 and 2.19, respectively (Table 1 and Figs. S5–S8 in ESI).

Device Fabrication

The devices were fabricated in the structure of ITO/PEDOT:PSS/active layer/PDINO/Ag. ITO-coated glass was sequentially sonically stirred in detergent, deionized water, acetone, dichloromethane and isopropanol. Then plasma treatment for 30 min. The PEDOT:PSS was spin-cast on the ITO glass with 4000 r/min for 30 s and annealed in air at 150 °C for 20 min.

https://doi.org/10.1007/s10118-023-3051-y

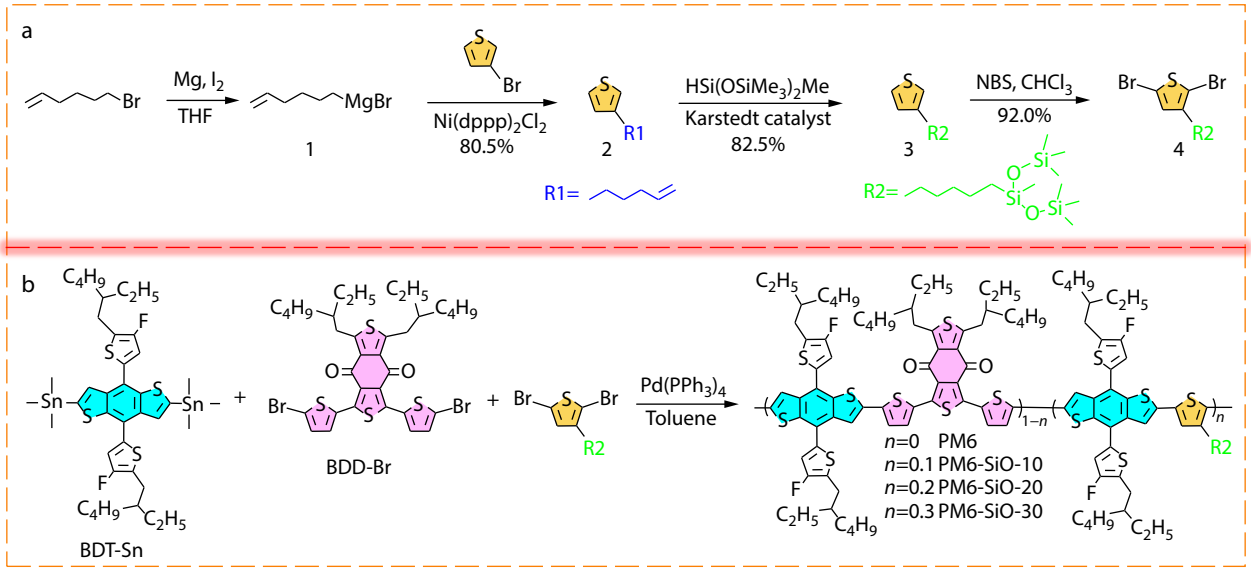

Fig. 1 Synthetic routes to siloxane-functionalized polymers.

Table 1 The molecular weight, optical properties and energy levels of the polymers.

Donor	M_n/PDI [a] (kDa/–)	λ_{max} [b]/λ_{max} [c] (nm)	λ_{onset} [c] (nm)	E_g [d] (eV)	HOMO/LUMO [e] (eV)	$I_{0\text{-}0}/I_{0\text{-}1}$	FWHM (nm)
PM6	35.35/2.04	618/622	674	1.84	–5.54/–3.70	1.05	141
PM6-SiO-10	30.51/2.23	616/622	674	1.84	–5.54/–3.70	1.05	146
PM6-SiO-20	35.95/2.18	612/618	674	1.84	–5.55/–3.71	1.04	152
PM6-SiO-30	34.94/2.19	612/618	674	1.84	–5.55/–3.71	1.04	152

[a] Determined by GPC at 150 °C (eluent: 1,2,4-trichlorobenzene); [b] Normalized maximum absorption peak in solutions; [c] Normalized maximum absorption peak and onset absorption in films; [d] Calculated from the formula: $E_g = 1240/\lambda_{onset}$; [e] Obtained from cyclic voltammetry (CV) method, $E_{LUMO} = E_{HOMO} + E_g$.

Subsequent operation of the device was done in a glove box filled with N_2. Chloroform dissolved the active layer material (PM6:Y6 weight ratio is 1:1.2) at a concentration of 16 mg·mL^{-1} with 0.5% 1-chloronaphthalene. The active layer solution was stirred at 40 °C for 3 h, then the active layer solution was spin-casted on the matrices with 3000 r/min. The thermal annealing of blend film is 100 °C for 10 min. Finally, 3 mg·mL^{-1} PDINO in methanol was spin-coated on the active layer. The device fabrication was accomplished by depositing 100 nm Ag in a vacuum chamber of 10^{-7} Torr. The device area of a typical cells is defined by a metal mask with an aperture aligned with the device area, which is 0.04 mm^2 in this experiment. The terpolymer:Y6 devices were prepared similar to that of PM6:Y6 device, except for the difference in weight ratio of donnor:acceptor (terpolymer:Y6=1:1, *W*:*W*). The optimize device parameters of PM6-SiO-10:Y6 are summarized in Table S1 (in ESI).

RESULTS AND DISCUSSION

Molecular Simulations

Ground state geometry optimization of PM6, PM6-SiO and PSiO was calculated by density function theory (DFT) at B3LYP/6-31g(d, p) level,[47] and the influence of thiophene unit on the polymer backbone was systematically studied. As shown in Fig. 2, with the increase of thiophene units (0%, 50%, 100%) in PM6, the dihedral angle (θ) of PM6, PM6-SiO and PSiO gradually increases, 9.55°, 25.59° and 26.18°, respectively, indicating that the introduction of thiophene units will destroy the coplanarity of the polymer backbone and need other functional groups such as siloxanes to compensate. The lowest unoccupied molecular orbital/highest occupied molecular orbital (LUMO/HOMO) of PM6, PM6-SiO and PSiO were calculated to be –2.61/–4.99, –2.52/–5.00 and –2.11/–5.01 eV, respectively, indicating that the introduction of thiophene units would slightly lower the HOMO energy level, pull up the LUMO energy level. From the molecular simulation results, it can be inferred that the introduction of siloxane-functionalized thiophene into PM6 will not significantly change the HOMO energy level. In addition, the incorporation of siloxane-functionalized thiophene unit could inevitable reduce the coplanarity of the molecular backbone with a certain extent. On the other hand, the unique structure of the siloxane which located away from the main chain's branch point and its large bulky nature, could enhances the π-π interaction, thereby preventing the loss of coplanarity.

Electrochemical and Optical Properties

The absorption spectra of PM6 and terpolymers in chloroform solution and thin film are shown in Fig. S9 (in ESI), Fig. 3(a) and Table 1. The absorption of siloxane-functionalized polymers is similar to that of PM6, the UV-Vis spectrum from solution to film state is redshifted by about 4 nm, the absorption edges of the film is 674 nm, and the optical band gap is 1.84 eV. With deepening the degree of the siloxane-functionalized polymer, the half-peak width (FWHM) of the absorption spectrum increases, and the absorption range becomes wider, which is conducive to improving the device J_{SC}. On the other hand, from the result of solution absorption spectra, it can be seen that the $\lambda_{0\text{-}0}/\lambda_{0\text{-}1}$ in-

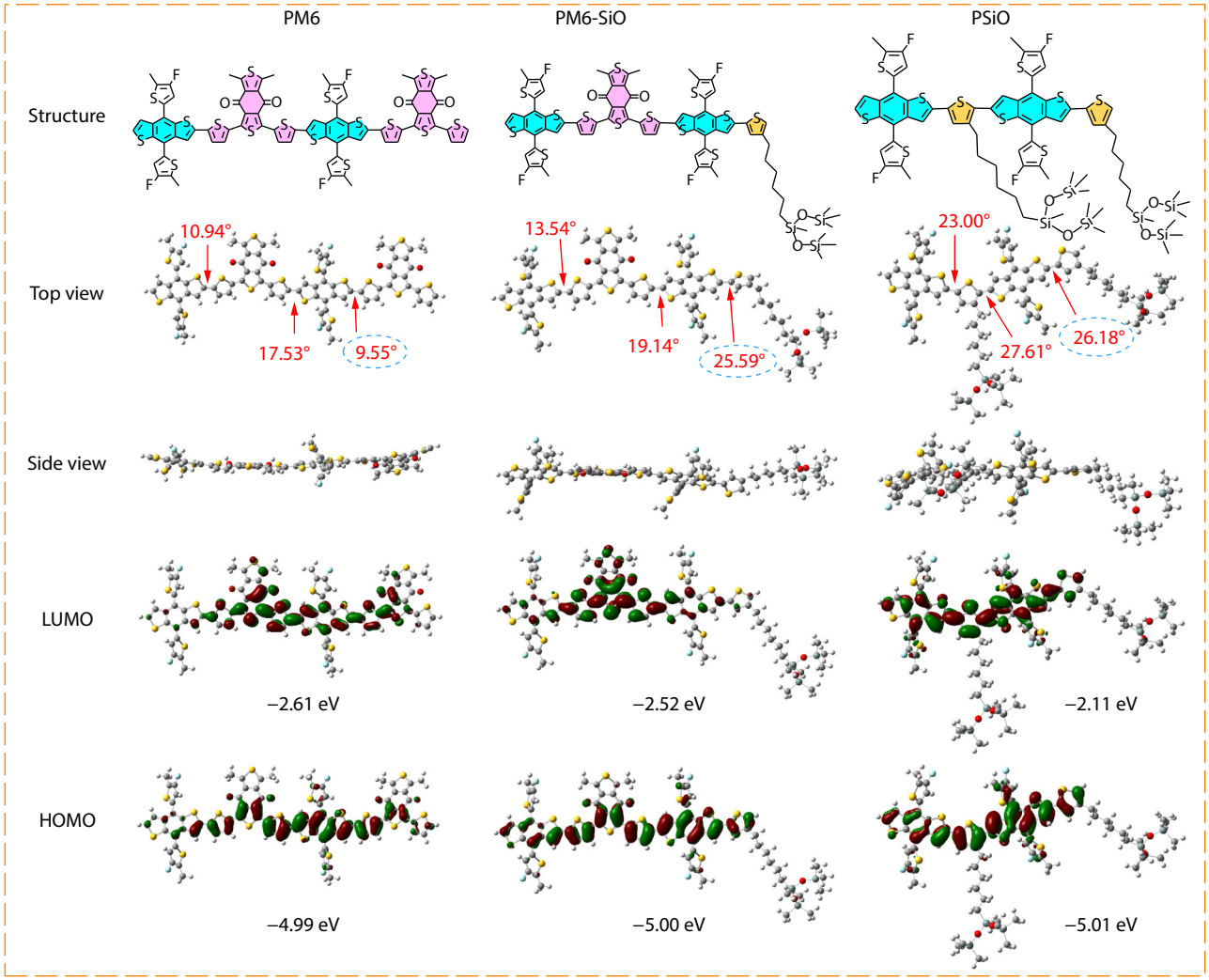

Fig. 2 Computational simulations of top view, side view, LUMO and HOMO for PM6, PM6-SiO and PSiO dimers.

tensity ratio of siloxane-functionalized polymers is smaller than PM6, indicating the decreased aggregation ability of siloxane-functionalized polymers. To further study the effect of siloxane-functionalized on polymer aggregation behavior, we tested the temperature-dependent absorption spectra of the four polymers (Figs. 3b–3e), and summarized the $\lambda_{0\text{-}0}/\lambda_{0\text{-}1}$ intensity ratio in Fig. S10 (in ESI). The results reveal that with the deepening of siloxane-functionalized, the aggregation ability of the polymers decreased, and the temperature-dependent ability increased, suggesting significant impact on the morphology of the active layer.

The HOMO energy levels of the four polymers were measured by cyclic voltammetry (CV) measurement, as shown in Fig. S11 (in ESI). The HOMO levels of PM6, PM6-SiO-10, PM6-SiO-20 and PM6-SiO-30 were calculated to be −5.54, −5.54, −5.55 and −5.55 eV, respectively. The LUMO levels of PM6, PM6-SiO-10, PM6-SiO-20 and PM6-SiO-30 were −3.70, −3.70, −3.71 and −3.71 eV, respectively, which calculated from the HOMO energy level and the corresponding optical band gap, as shown in Fig. 3(f) and Table 1. With the increase of the siloxane-functionalized thiophene unit, the energy level of the ternary polymer changes slightly, indicating that the siloxane-functionalized method could not affect the matching of the energy levels between donor and acceptor.

Device Characteristics

To investigate the effect of siloxane-functionalized unit on the photovoltaic performance of polymers, OSCs with device structure of ITO/PEDOT:PSS/Polymer:Y6/PDINO/Ag were prepared, and the corresponding preparation process was presented in ESI. Fig. 4(a) exhibits the density-voltage (*J-V*) curves of the optimal devices for PM6:Y6, PM6-SiO-10:Y6, PM6-SiO-20:Y6 and PM6-SiO-30:Y6, and the related parameters were summarized in Table 2. We optimized the performance of siloxane-functionalized polymer-based devices by changing the D:A ratio, the concentration of active layer and thermal annealing time, *etc.* (Table S1 in ESI). In these polymers, the incorporation of a 10% molar siloxane-functionalized unit gave the best device performance. The device based on PM6-SiO-10:Y6 demonstrated the optimal performance, achieving the highest PCE of 16.69%. This remarkable efficiency was accompanied by a high V_{OC} of 0.850 V, an impressive J_{SC} of 26.96 mA·cm^{-2}, and an FF of 72.84%. In comparison, the counterparts PM6:Y6, PM6-SiO-20:Y6, and PM6-SiO-30:Y6 exhibited relatively lower PCE values. It is worth not-

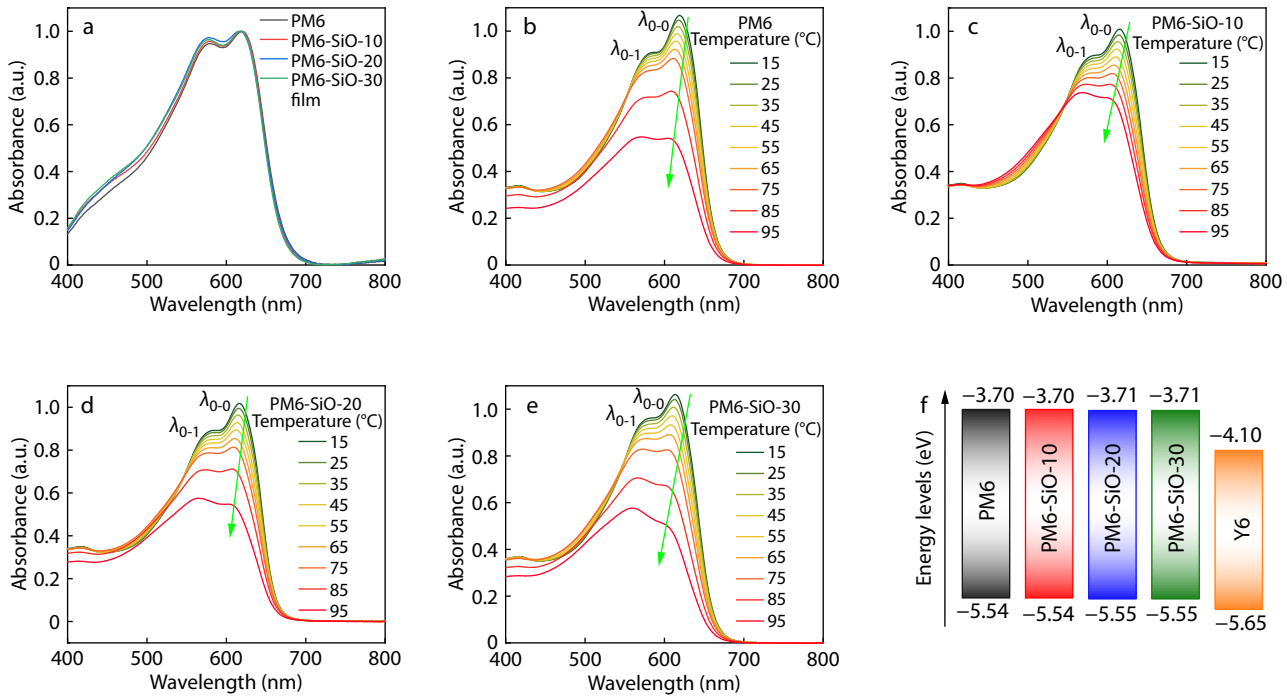

Fig. 3 (a) The absorption spectra in pure film of the polymers; The absorption spectra of (b) PM6, (c) PM6-SiO-10, (d) PM6-SiO-20 and (e) PM6-SiO-30 in chlorobenzene from 95 °C to 15 °C as indicated, arrows indicate the spectral trend with increasing temperature; (f) The energy level diagram of the polymers and Y6.

ing that the PCE of 16.69% is one of the highest values reported by binary OSCs based on siloxane-functionalized polymer to date (Fig. 4b and Table S2 in ESI). The best J_{SC} in PM6-SiO-10:Y6-based OSCs may be due to the improved morphology by introducing appropriate ratios of siloxane-functionalized thiophene, which will be discussed later. To confirm the batch reproducibility of the siloxanized terpolymer, we synthesized other two batches of PM6-SiO-10 and studied their photovoltaic performance. As shown in Fig. S12 and Table S3 (in ESI), the three batches of PM6-SiO-10 with various molecular weights could maintain high PCEs over 16.5%, indicating the good batch reproducibility of the terpolymers. The external quantum efficiency (EQE) spectra of these devices were presented in Fig. 4(c), and the corresponding integral J_{SC} were 25.07, 26.13, 25.48 and 25.22 mA·cm^{-2}, respectively, which agree well with the result form *J-V* curves. PM6-SiO-10-based devices maintain high EQE response in the range of 350–900 nm.

We further studied the thermal and light stability of PM6:Y6, PM6-SiO-10:Y6, PM6-SiO-20:Y6 and PM6-SiO-30:Y6 device. Through the stability testing of the optimal OSCs devices, we found that the thermal and light stability of PM6-Si0-10:Y6-based device both improved compared with PM6:Y6 counterpart, as shown in Fig. S13 and Fig. S14 (in ESI), respectively. Moreover, there is a tendency for higher siloxane content to correspond to improved stability. We inferred that the following two reasons may lead to its increased stability. First, the presence of bulky siloxane groups with steric hindrance effects limits chain migration, hinders thermal motion, and results in improved thermal stability. Second, The bond energy of Si—O is greater than that of C—C, which helps to resist radiation and obtain better light stability. This can improve the intrinsic stability of the material, and thus improving the stability of the corresponding device.

The *J-V* curve was measured at different light intensities to study the charge recombination behaviors of the devices. The J_{SC} depend on light intensity curve were shown in Fig. 4(d). In general, the relationship between light intensity (P_{light}) and J_{SC} is $J_{SC} \propto P_{light}^{\alpha}$, where α=1 indicates the collection of free carriers without charge recombination, and α<1 indicates the presence of some degree of bimolecular recombination.[48–50] The α of PM6:Y6, PM6-SiO-10:Y6, PM6-SiO-20:Y6 and PM6-SiO-30:Y6-based devices were all close to 0.879, indicating that the siloxane-functionalized method proposed in this work does not affect the bimolecular recombination of polymers. On the other hand, On the other hand, according to the relationship of $V_{OC} \propto n(kT/q)\ln P_{light}$ (where T, k and q are the Kelvin temperature, Boltzmann constant and elementary charge, respectively), the slope S of the V_{OC} to $\ln P_{light}$ fitting curve can be established. And when S close to 2 kT/q indicates that the device is dominated by trap-assisted recombination, and S close to 1 kT/q means that the device is dominated by bimolecular recombination.[48–50] As shown in Fig. 4(e), the S of PM6:Y6, PM6-SiO-10:Y6, PM6-SiO-20:Y6 and PM6-SiO-30:Y6 devices were calculated to be 1.24, 1.19, 1.30 and 1.25 kT/q, respectively. The S of these devices is close to 1 kT/q, indicating that the trap-assisted recombination of the device is relatively weak. Among them, the trap-assisted recombination is weakest when the 10% molar siloxane-functionalized unit is incorporated.

To better understand the exciton dissociation and charge collection characteristics in these devices, the effective photocurrent density (J_{ph}) versus effective voltage (V_{eff}) curve was plotted,[51] where J_{ph} and V_{eff} are defined as $J_{ph} = J_L - J_D$ and $V_{eff} = V_0 - V_{bias}$, respectively (where J_L, J_D, V_0 and V_{bias} corre-

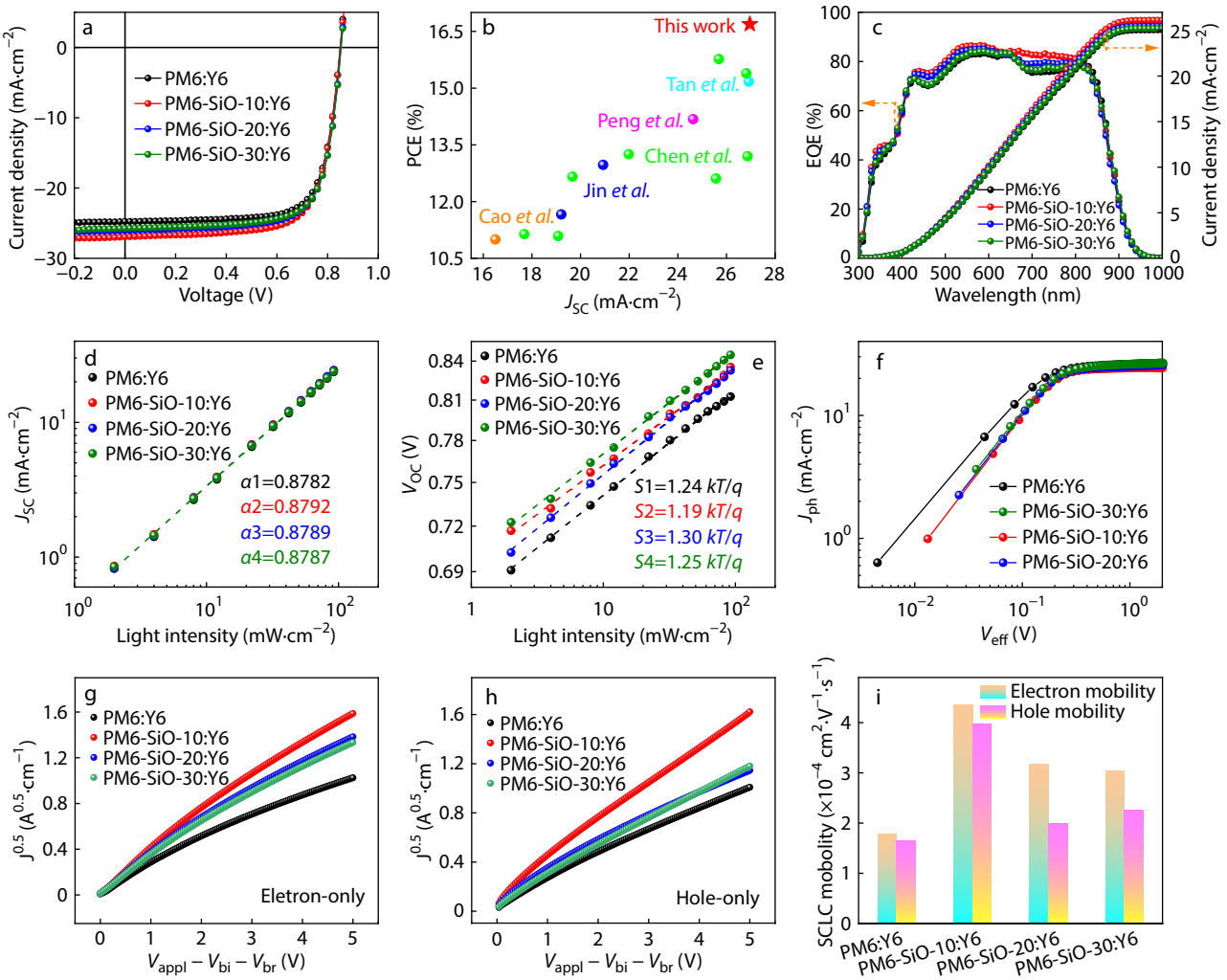

Fig. 4 (a) Current density versus voltage (*J-V*) curves of organic solar cells based on terpolymers and PM6; (b) A brief summary of PCE versus J_{SC} for binary OSCs of siloxane-functionalized polymers in this work and literatures; (c) EQE spectra and relevant integrated J_{SC}; The dependence of J_{SC} (d) and V_{OC} (e) on the light intensity; J_{ph}-V_{eff} curves (f), plots for the measurements of electron mobilities (g) and hole mobilities (h), the determined carrier mobilities (i) of PM6:Y6, PM6-SiO-10:Y6 PM6-SiO-20:Y6 and PM6-SiO-30:Y6-based devices.

Table 2 Photovoltaic parameters of polymers:Y6-based devices under simulated AM 1.5 G (100 mW·cm^{-2}) illumination.

Active layer	V_{OC} (V)	J_{SC} (mA·cm^{-2})	FF (%)	PCE [a] (%)
PM6:Y6	0.848(0.849±0.005)	25.57(25.61±0.30)	72.13(71.84±0.22)	15.64(15.32±0.32)
PM6-SiO-10:Y6	0.850(0.853±0.005)	26.96(26.60±0.42)	72.84(73.26±0.53)	16.69(16.24±0.45)
PM6-SiO-20:Y6	0.852(0.853±0.006)	26.07(25.72±0.40)	72.16(72.04±0.26)	16.03(15.79±0.38)
PM6-SiO-30:Y6	0.853(0.853±0.008)	25.72(25.66±0.27)	72.15(71.93±0.25)	15.82(15.58±0.34)

[a] Average PCEs in brackets for over 20 devices.

spond to in the light, in the dark, J_{ph} = 0 and the applied voltage).[4] As shown in Fig. 4(f) and Table S4 (in ESI), J_{ph} reaches saturation (J_{sat}) when V_{eff}>2 V, indicative of that the internal electric field is sufficient to collect all charge carriers.[52] Exciton dissociation efficiency (P_{diss}) and charge collection efficiency (P_{coll}) can be determined by the values of J_{ph}/J_{sat}.[53,54] The P_{diss} of PM6:Y6, PM6-SiO-10:Y6, PM6-SiO-20:Y6 and PM6-SiO-30:Y6 were calculated to be 97.51%, 99.83%, 97.48% and 97.01%, respectively. In addition, the P_{coll} of PM6-SiO-10:Y6 (89.46%) was higher than PM6:Y6 (82.50%), PM6-SiO-20:Y6 (86.22%), and PM6-SiO-30:Y6 (86.22%). The changes in P_{diss} and P_{coll} are consistent with the corresponding device performance.

The siloxane-functionalized polymer also affects the charge transport characteristics, thus we further investigated the charge carrier mobility of the blended film by using the space charge limited current (SCLC) model, and the results were shown in Figs. 4(g)–4(i) and Table S4 (in ESI). The device structures for testing electron mobility (μ_e) and hole mobility (μ_h) were ITO/ZnO/active layer/PDINO/Ag and ITO/PEDOT:PSS/active layer/MoO_3/Ag, respectively. The μ_e/μ_h of PM6:Y6, PM6-SiO-10:Y6, PM6-SiO-20:Y6 and PM6-SiO-30:Y6 are

$1.79\times10^{-4}/1.65\times10^{-4}$, $4.36\times10^{-4}/3.98\times10^{-4}$, $3.17\times10^{-4}/1.99\times10^{-4}$ and $3.04\times10^{-4}/2.25\times10^{-4}$ $cm^2\cdot V^{-1}\cdot s^{-1}$, and the corresponding μ_e/μ_h ratios are 1.08, 1.10, 1.59 and 1.35, respectively. These results are indicative of that the PM6-SiO-10:Y6 blend exhibits the highest and most balanced charge mobility, which is conducive to the improvement of J_{SC} and FF. Furthermore, in order to better evaluate the charge transport performance of polymers, we investigated the hole mobility of PM6, PM6-SiO-10, PM6-SiO-20 and PM6-SiO-30 in neat film by using the SCLC model, and the results were 7.56×10^{-4}, 14.98×10^{-4}, 12.59×10^{-4} and 8.28×10^{-4} $cm^2\cdot V^{-1}\cdot s^{-1}$, respectively (Fig. S15 in ESI), indicating that appropriate amount of siloxane-functionalized thiophene into polymer can significantly improve the hole transport performance. Finally, we also measured the fluorescence quenching efficiency of PM6:Y6, PM6-SiO-10:Y6, PM6-SiO-20:Y6 and PM6-SiO-30:Y6 blended films by steady-state fluorescence spectroscopy, as shown in Fig. 5 and Table S4. Under the condition of donor excitation wavelength of 570 nm (P_D, Figs. 5a–5d) and acceptor excitation wavelength of 830 nm (P_A, Figs. 5e–5h), the fluorescence quenching efficiency of PM6-SiO-10:Y6 blend (98.24%/98.95%) was better than that of PM6:Y6 (98.00%/95.70%), PM6-SiO-20:Y6 (97.58%/94.19%) and PM6-SiO-30:Y6 (96.20%/93.02%), confirming more efficient charge transfer in PM6-SiO-10:Y6 blend.

Effect of Siloxane-functionalized Unit on the Crystallinity of Polymers

To further understand polymer aggregation properties in the film, the grazing-incidence wide-angle X-ray scattering (GIWAXS) of PM6, PM6-SiO-10, PM6-SiO-20, PM6-SiO-30 pure films and blend films were conducted, as shown in Figs. 6(a)–6(d) and Figs. 6(e)–6(h), respectively. Fig. 6(i) describes the integration curves of the corresponding film in the out-of-plane (OOP, solid) and in-plane (IP, dashed) and summarizes the corresponding parameters in Table 3. The (100) diffraction peaks in the IP direction of PM6, PM6-SiO-10, PM6-SiO-20 and PM6-SiO-30 pure films were located at 0.285, 0.283, 0.280 and 0.277 $Å^{-1}$, respectively, and the crystalline coherence length (CCL) corresponding to lamellar stacking were 44.93, 43.10, 42.94 and 42.63 Å, respectively. The above result indicates that the increased content of siloxane-functionalized thiophene of the polymer, the weaker crystallinity of the lamellar stacked in the IP direction. In addition, PM6:Y6, PM6-SiO-10:Y6, PM6-SiO-20:Y6 and PM6-SiO-30:Y6 blend films showed similar trend in crystallinity as pure films, indicating that the siloxane-functionalized thiophene slightly disrupted the crystallinity and arrangement of the polymer in the IP direction. This is mainly due to the disordered arrangement of polymer backbone induced by ternary random copolymerization. Interestingly, the crystallinity of PM6, PM6-SiO-10, PM6-SiO-20 and PM6-SiO-30 pure films in the OOP di-

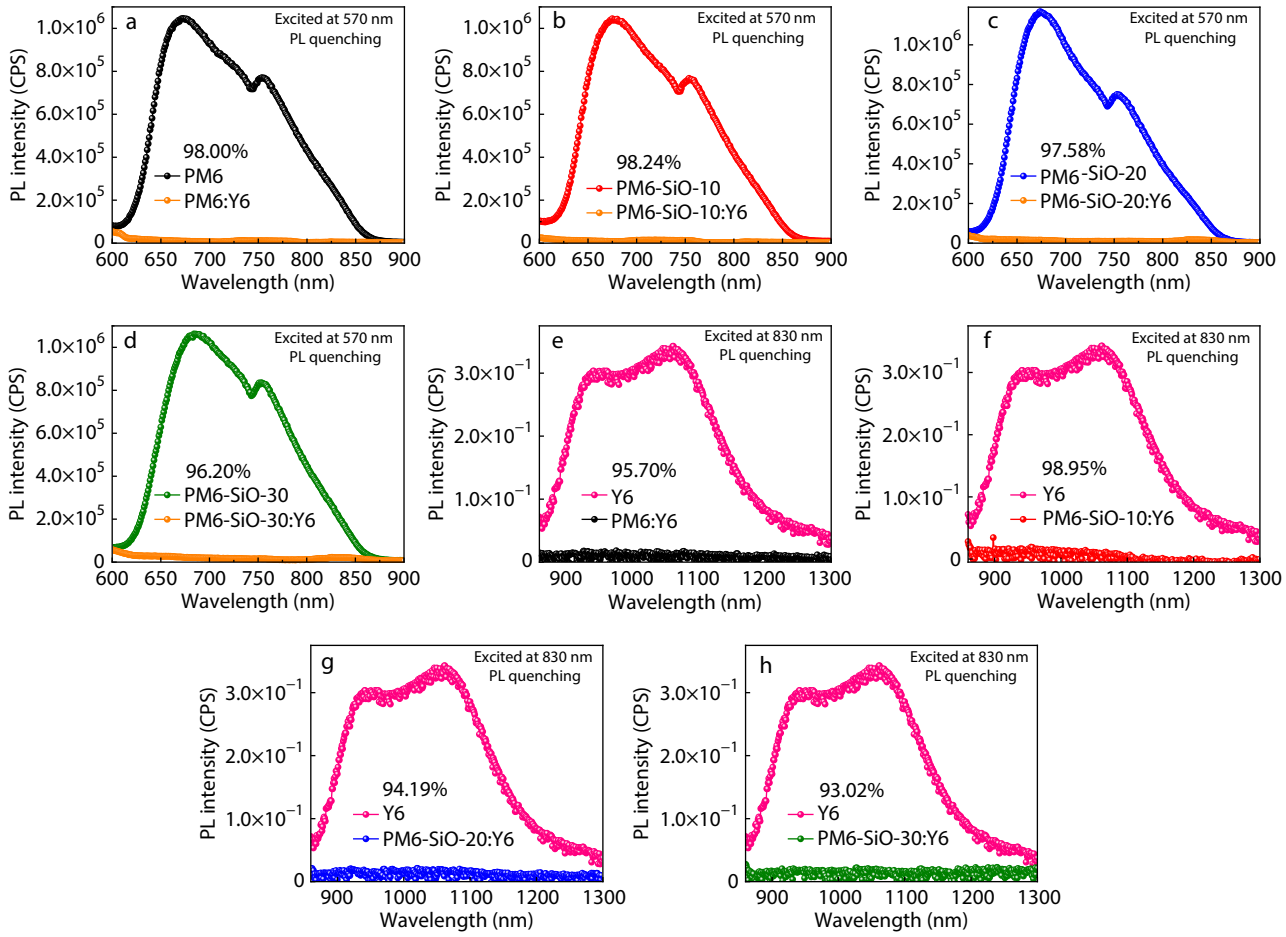

Fig. 5 The steady-state fluorescence spectra of the corresponding blend films at the excitation wavelength of 570 nm (a–d) and the excitation wavelength of 830 nm (e–h).

https://doi.org/10.1007/s10118-023-3051-y

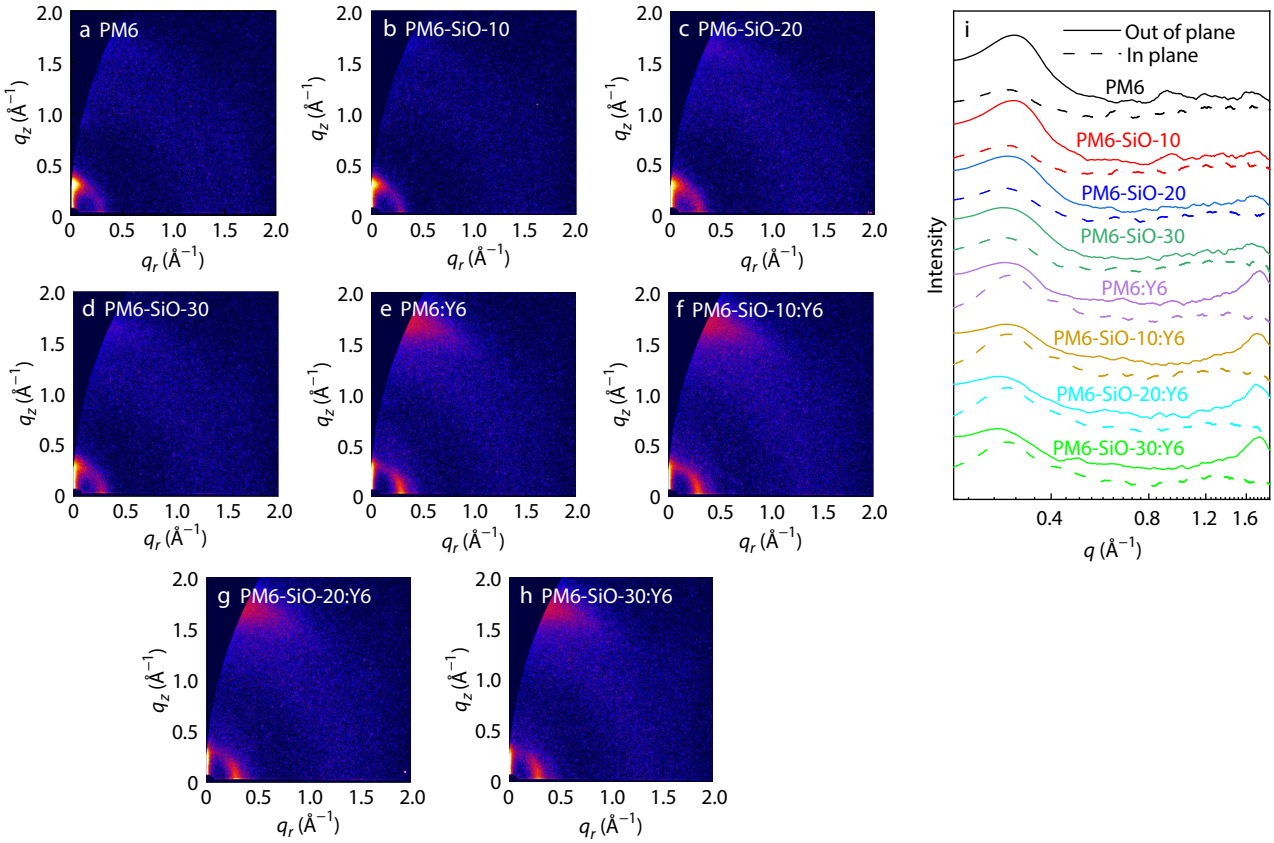

Fig. 6 Two-dimensional GIWAXS images of the (a) PM6, (b) PM6-SiO-10, (c) PM6-SiO-20, (d) PM6-SiO-30, (e) PM6:Y6, (f) PM6-SiO-10:Y6, (g) PM6-SiO-20:Y6, and (h) PM6-SiO-30:Y6; (i) Corresponding one-dimensional intensity profiles in the in plane (IP) and out of plane (OOP) direction.

Table 3 Summarized parameters for the ordering structures of films in GIWAXS.

Material	In plane (lamellar)			Out of plane (π-π)		
	100 (Å^{-1})	d (Å)	CCL (Å)	010 (Å^{-1})	d (Å)	CCL (Å)
PM6	0.285	22.04	44.93	1.655	3.79	18.25
PM6-SiO-10	0.283	22.19	43.10	1.657	3.79	5.03
PM6-SiO-20	0.280	22.43	42.94	1.644	3.82	8.93
PM6-SiO-30	0.277	22.67	42.63	1.639	3.83	12.30
PM6:Y6	0.299	21.00	73.10	1.744	3.60	25.39
PM6-SiO-10:Y6	0.295	21.29	69.94	1.728	3.63	24.34
PM6-SiO-20:Y6	0.294	21.29	69.94	1.727	3.64	24.85
PM6-SiO-30:Y6	0.292	21.51	63.00	1.726	3.64	25.17

rection have different trends, and the (010) diffraction peaks are located at 1.655, 1.657, 1.644 and 1.639 Å^{-1}, corresponding to π-π stacking and the CCLs are calculated to be 18.25, 5.03, 8.93 and 12.30 Å, respectively. The results show that the crystallinity of the random copolymerized terpolymers decreased suddenly compared to that of the binary alternating polymer PM6, which may be attribute to the increased disorder of the backbone in terpolymers. Nevertheless, with the further increase of siloxane-functionalized unit, the π-π interaction of the polymer chain was enhanced, the disorder caused by random copolymerization is inhibited, and π-π stacking in the OOP direction is further improved. Therefore, the siloxane-functionalized side chain weakens the lamellar interaction while enhancing the π-π interaction, which contributes to the face-on orientation of the polymer chain. The change of crystallinity in PM6:Y6, PM6-SiO-10:Y6, PM6-SiO-20:Y6 and PM6-SiO-30:Y6 blends in the OOP direction was consistent with that of the pure film, indicating that the siloxane-functionalized unit can significantly affect the crystallinity of the whole active layer, which in turn affects the mobility and J_{SC} of the device.

Effect of Siloxane-functionalized on Morphology of Active Layer

To further elucidate the impact of siloxane-functionalized side chains on the film-forming process, we conducted color mapping of *in situ* UV-Vis absorption spectra while varying the spin-coating time. This was performed using high-boiling chlorobenzene as the solvent. As shown in Fig. S16 (in ESI), the film-forming time of PM6 and PM6-SiO-10 are almost the same, at 15.72 s and 15.63 s, respectively. However, their diffusion rates differ, with PM6 diffusing more faster than PM6-SiO-10, illustrating their different morphology of the active layer. To gain deep in-

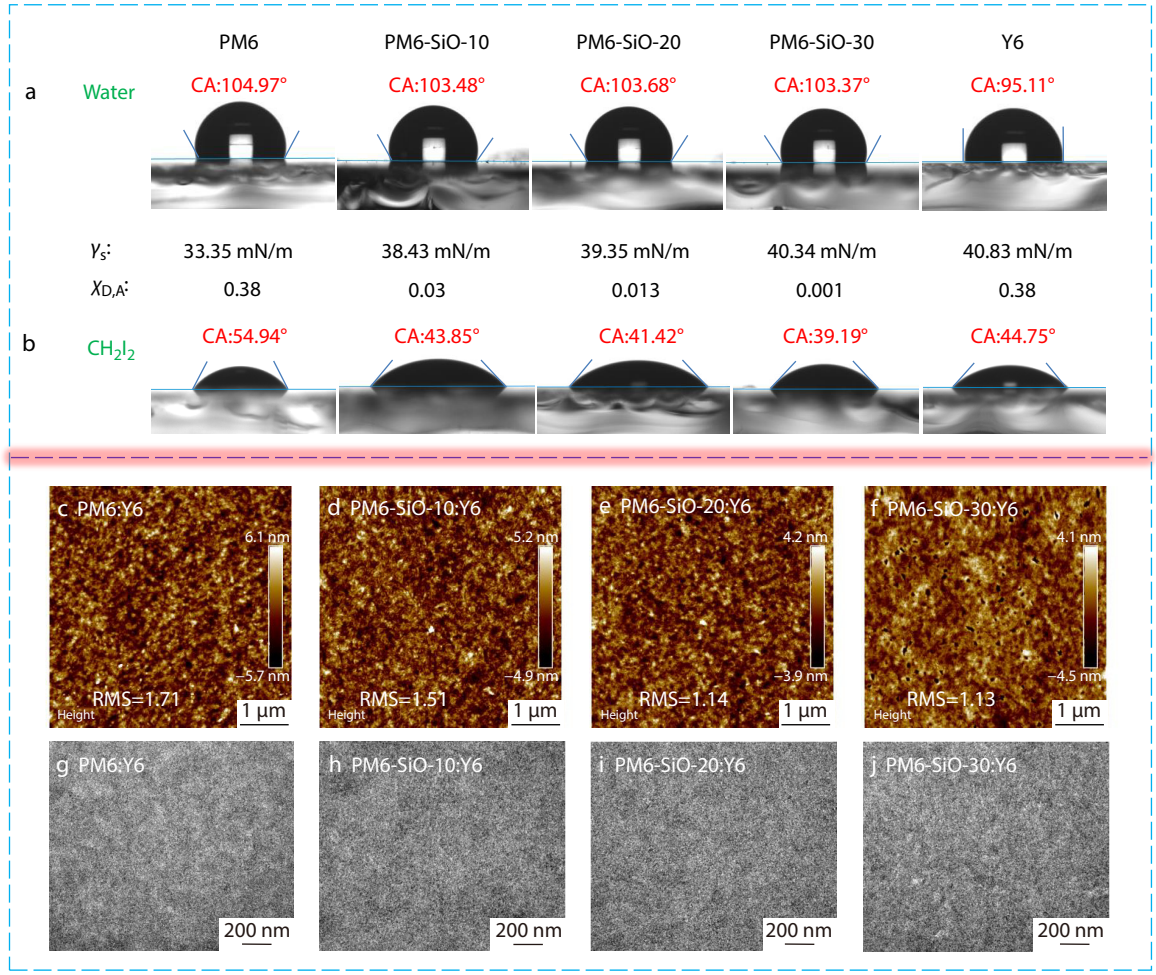

Fig. 7 (a) Water and (b) CH_2I_2 contact angle of PM6, PM6-SiO-10, PM6-SiO-20, PM6-SiO-30 and Y6. (c–f) AFM and (g–j) TEM images of blend films based on siloxane-functionalized polymers and PM6.

sights into the effect of siloxane-functionalized on the phase separation in active layer, water and diiodomethane biphasic contact angle of PM6, PM6-SiO-10, PM6-SiO-20, PM6-SiO-30 and Y6 were performed. As shown in Figs. 7(a) and 7(b), with the increase of siloxane-functionalized units, the surface tension (γ_s) increases, and the Flory-Huggins interaction parameter ($\chi_{D\text{-}A}$) decreases, indicating the miscibility increased. Besides, in comparison to PM6, the γ_s and $\chi_{D\text{-}A}$ of terpolymer PM6-SiO-10 from random polymerization decreased dramatically. When the content of siloxane-functionalized units further increase, the γ_s and $\chi_{D\text{-}A}$ tended to be maintain, indicating that the changes of γ_s and $\chi_{D\text{-}A}$ were mainly caused by disorder of random copolymerization, and further increase of siloxane-functionalized unit content would enhance the π-π interaction and inhibit disorder. Moreover, the surface morphology of PM6:Y6, PM6-SiO-10:Y6, PM6-SiO-20:Y6, and PM6-SiO-30:Y6 blend films were carefully studied by atomic force microscopy (AFM) and transmission electron microscopy (TEM), as shown in Figs. 7(c)–7(j). The root means square (RMS) roughness values of PM6:Y6, PM6-SiO-10:Y6, PM6-SiO-20:Y6 and PM6-SiO-30:Y6 were 1.71, 1.51, 1.14 and 1.13 nm, respectively, indicating that the phase separation between donor and acceptor was weakened with the increase of siloxane-functionalized unit, which was also consistent with the contact angle and TEM test results. The polymer PM6-SiO-10 based on 10% siloxane functionalization unit obtains the best active layer morphology, and when the content of the siloxane functionalized unit is too large, the miscibility between donor and acceptor is too good and leads to overmixing, leading to increased trap-assisted recombination, which is detrimental to achieving high-performance OSCs.

CONCLUSIONS

In conclusion, a novel siloxane-functionalized thiophene unit was developed and incorporated into the PM6 backbone to obtain a series of terpolymers (PM6-SiO-10, PM6-SiO-20 and PM6-SiO-30) by random polymerization. The siloxane-functionalized unit has negligible effect on energy level and absorption of the polymer, while significantly influence the molecular aggregation and thereby could change the active layer morphology and device performance. Interestingly, the unique structure of siloxane, located away from the main chain's branch point and having a bulky nature, enhances the π-π interaction within the polymer chain and suppresses the disorder caused by random copolymerization. When the content of siloxane-functionalized units over 10%, the π-π stacking in OOP direction increased along with the lamellar interaction in the IP direction weakened, illustrating the improvement of face-on orientation of the ter-

https://doi.org/10.1007/s10118-023-3051-y

polymers, which is favorable for charge transport. Compared to PM6-SiO-20:Y6 and PM6-SiO-30:Y6 system, PM6-SiO-10:Y6 based device exhibited large and more balanced hole and electron mobility, more efficient charge collection and less charge recombination. As a result, the PM6-SiO-10:Y6 based device exhibited the highest PCE of 16.69% with a V_{OC} of 0.850 V, a J_{SC} of 26.96 mA·cm^{-2} and an FF of 72.84%. This work offers new possibilities for fine-tuning the crystallinity and morphology of polymers in OSCs, providing valuable insights for future research.

Conflict of Interests

The authors declare no interest conflict.

Electronic Supplementary Information

Electronic supplementary information (ESI) is available free of charge in the online version of this article at http://doi.org/10.1007/s10118-023-3051-y.

ACKNOWLEDGMENTS

This work was financially supported by the National Natural Science Foundation of China (NSFC) (Nos. 51973032, 21905043, 51833004 and 52333006), the Jiangxi Provincial Natural Science Foundation (Nos. 20212ACB203005, 20224ACB214002, 20212BAB213018 and 20224BAB203015), the Thousand Talents Plan of Jiangxi Province (No. jxsq2019101051), and the Innovation Foundation for graduate students of Jiangxi Normal University (No. YJS2021018). X.X. and X.L. acknowledge the financial support from Research Grants Council (RGC) of Hong Kong (General Research Fund No. 14303519).

REFERENCES

1 Yu, G.; Gao, J.; Hummelen, J. C.; Wudl, F.; Heeger, A. J. Polymer photovoltaic cells: enhanced efficiencies *via* a network of internal donor-acceptor heterojunctions. *Science* **1995**, *270*, 1789–1791.
2 Zhang, G.; Lin, F. R.; Qi, F.; Heumüller, T.; Distler, A.; Egelhaaf, H. J.; Li, N.; Chow, P. C. Y.; Brabec, C. J.; Jen, A. K. Y.; Yip, H. L. Renewed prospects for organic photovoltaics. *Chem. Rev.* **2022**, *122*, 14180–14274.
3 Li, S.; Li, Z.; Wan, X.; Chen, Y. Recent progress in flexible organic solar cells. *eScience* **2023**, *3*, 100085.
4 Xie, Q.; Liu, Y.; Liao, X.; Cui, Y.; Huang, S.; Hu, L.; He, Q.; Chen, L.; Chen, Y. Isomeric effect of wide bandgap polymer donors with high crystallinity to achieve efficient polymer solar cells. *Macromol. Rapid Commun.* **2020**, *41*, e2000454.
5 Cui, Y.; Zhu, P.; Xia, X.; Lu, X.; Liao, X.; Chen, Y. Carbazolebis(thiadiazole)-core based non-fused ring electron acceptors for efficient organic solar cells. *Chin. Chem. Lett.* **2023**, *34*, 107902.
6 Xu, G.; Hu, X.; Liao, X.; Chen, Y. Bending-stability interfacial layer as dual electron transport layer for flexible organic photovoltaics. *Chinese J. Polym. Sci.* **2021**, *39*, 1441–1447.
7 Wu, M.; Shi, L.; Hu, Y.; Chen, L.; Hu, T.; Zhang, Y.; Yuan, Z.; Chen, Y. Additive-free non-fullerene organic solar cells with random copolymers as donors over 9% power conversion efficiency. *Chin. Chem. Lett.* **2019**, *30*, 1161–1167.
8 Yuan, J.; Zhang, Y.; Zhou, L.; Zhang, G.; Yip, H. L.; Lau, T. K.; Lu, X.; Zhu, C.; Peng, H.; Johnson, P. A.; Leclerc, M.; Cao, Y.; Ulanski, J.; Li, Y.; Zou, Y. Single-junction organic solar cell with over 15% efficiency using fused-ring acceptor with electron-deficient core. *Joule* **2019**, *3*, 1140–1151.
9 Jiang, K.; Wei, Q.; Lai, J.; Peng, Z.; Kim, H.; Yuan, J.; Ye, L.; Ade, H.; Zou, Y.; Yan, H. Alkyl chain tuning of small molecule acceptors for efficient organic solar cells. *Joule* **2019**, *3*, 3020–3033.
10 Wang, J. L.; Wang, L.; An, Q.; Yan, L.; Bai, H. R.; Jiang, M.; Mahmood, A.; Yang, C.; Zhi, H. Non-fullerene acceptors with hetero-dihalogenated terminals induce significant difference in single crystallography and enable binary organic solar cells with 17.5% efficiency. *Energy Environ. Sci.* **2022**, *15*, 320–333.
11 Luo, Z.; Ma, R.; Chen, Z.; Xiao, Y.; Zhang, G.; Liu, T.; Sun, R.; Zhan, Q.; Zou, Y.; Zhong, C.; Chen, Y.; Sun, H.; Chai, G.; Chen, K.; Guo, X.; Min, J.; Lu, X.; Yang, C.; Yan, H. Altering the positions of chlorine and bromine substitution on the end group enables high-performance acceptor and efficient organic solar cells. *Adv. Energy Mater.* **2020**, *10*, 2002649.
12 Cheng, F.; Cui, Y.; Ding, F.; Chen, Z.; Xie, Q.; Xia, X.; Zhu, P.; Lu, X.; Zhu, H.; Liao, X.; Chen, Y. Terpolymerization and regioisomerization strategy to construct efficient terpolymer donors enabling high-performance organic solar cells. *Adv. Mater.* **2023**, e2300820.
13 Liu, Y.; Liu, B.; Ma, C. Q.; Huang, F.; Feng, G.; Chen, H.; Hou, J.; Yan, L.; Wei, Q.; Luo, Q.; Bao, Q.; Ma, W.; Liu, W.; Li, W.; Wan, X.; Hu, X.; Han, Y.; Li, Y.; Zhou, Y.; Zou, Y.; Chen, Y.; Li, Y.; Chen, Y.; Tang, Z.; Hu, Z.; Zhang, Z. G.; Bo, Z. Recent progress in organic solar cells (Part I material science). *Sci. China Chem.* **2021**, *65*, 224–268.
14 Xu, X.; Zhang, G.; Yu, L.; Li, R.; Peng, Q. P3HT-based polymer solar cells with 8.25% efficiency enabled by a matched molecular acceptor and smart green-solvent processing technology. *Adv. Mater.* **2019**, *31*, e1906045.
15 Xu, X.; Li, Y.; Peng, Q. Ternary blend organic solar cells: understanding the morphology from recent progress. *Adv. Mater.* **2022**, *34*, e2107476.
16 Zhu, L.; Zhang, M.; Xu, J.; Li, C.; Yan, J.; Zhou, G.; Zhong, W.; Hao, T.; Song, J.; Xue, X.; Zhou, Z.; Zeng, R.; Zhu, H.; Chen, C. C.; MacKenzie, R. C. I.; Zou, Y.; Nelson, J.; Zhang, Y.; Sun, Y.; Liu, F. Single-junction organic solar cells with over 19% efficiency enabled by a refined double-fibril network morphology. *Nat. Mater.* **2022**, *21*, 656–663.
17 Zheng, Z.; Wang, J.; Bi, P.; Ren, J.; Wang, Y.; Yang, Y.; Liu, X.; Zhang, S.; Hou, J. Tandem organic solar cell with 20.2% efficiency. *Joule* **2022**, *6*, 171–184.
18 Xu, X.; Yu, L.; Meng, H.; Dai, L.; Yan, H.; Li, R.; Peng, Q. Polymer solar cells with 18.74% efficiency: from bulk heterojunction to interdigitated bulk heterojunction. *Adv. Funct. Mater.* **2021**, *32*, 2108797.
19 Pang, B.; Liao, C.; Xu, X.; Peng, S.; Xia, J.; Guo, Y.; Xie, Y.; Chen, Y.; Duan, C.; Wu, H.; Li, R.; Peng, Q. B-N bond embedded triplet terpolymers with small singlet-triplet energy gaps for suppressing non-radiative recombination and improving blend morphology in organic solar cells. *Adv. Mater.* **2023**, e2211871.
20 Lu, H.; Liu, W.; Jin, H.; Huang, H.; Tang, Z.; Bo, Z. High-efficiency organic solar cells with reduced nonradiative voltage loss enabled by a highly emissive narrow bandgap fused ring acceptor. *Adv. Funct. Mater.* **2021**, *32*, 2107756.
21 Chong, K.; Xu, X.; Meng, H.; Xue, J.; Yu, L.; Ma, W.; Peng, Q. Realizing 19.05% efficiency polymer solar cells by progressively improving charge extraction and suppressing charge recombination. *Adv. Mater.* **2022**, *34*, e2109516.
22 Zhang, Z. G.; Bai, Y.; Li, Y. Benzotriazole based 2D-conjugated polymer donors for high performance polymer solar cells. *Chinese J. Polym. Sci.* **2021**, *39*, 1–13.
23 Chen, S.; Yao, H.; Li, Z.; Awartani, O. M.; Liu, Y.; Wang, Z.; Yang, G.; Zhang, J.; Ade, H.; Yan, H. Surprising effects upon inserting benzene units into a quaterthiophene-based D-A polymer-improving non-fullerene organic solar cells via donor polymer design. *Adv. Energy Mater.* **2017**, *7*, 1602304.
24 Li, S.; Ye, L.; Zhao, W.; Yan, H.; Yang, B.; Liu, D.; Li, W.; Ade, H.; Hou,

J. A wide band gap polymer with a deep highest occupied molecular orbital level enables 14.2% efficiency in polymer solar cells. *J. Am. Chem. Soc.* **2018**, *140*, 7159–7167.
25 Zhang, M.; Guo, X.; Ma, W.; Ade, H.; Hou, J. A large-bandgap conjugated polymer for versatile photovoltaic applications with high performance. *Adv. Mater.* **2015**, *27*, 4655–4660.
26 Zheng, Z.; Yao, H.; Ye, L.; Xu, Y.; Zhang, S.; Hou, J. PBDB-T and its derivatives: a family of polymer donors enables over 17% efficiency in organic photovoltaics. *Mater. Today* **2020**, *35*, 115–130.
27 Liu, D.; Wang, J.; Gu, C.; Li, Y.; Bao, X.; Yang, R. Stirring up acceptor phase and controlling morphology *via* choosing appropriate rigid aryl rings as lever arms in symmetry-breaking benzodithiophene for high-performance fullerene and fullerene-free polymer solar cells. *Adv. Mater.* **2018**, *30*, 1705870.
28 Jin, K.; Xiao, Z.; Ding, L. D18, an eximious solar polymer! *J. Semicond.* **2021**, *42*, 010502.
29 Jiang, H.; Qin, G.; Zhang, L.; Pan, F.; Wu, Z.; Wang, Q.; Wen, G.; Zhang, W.; Cao, Y.; Chen, J. Dithienobenzoxadiazole-based wide bandgap donor polymers with strong aggregation properties for the preparation of efficient as-cast non-fullerene polymer solar cells processed using a non-halogenated solvent. *J. Mater. Chem. C* **2021**, *9*, 249–259.
30 Xie, R.; Ying, L.; An, K.; Zhong, W.; Yin, Q.; Liao, S.; Huang, F.; Cao, Y. Efficient non-fullerene organic solar cells based on a wide-bandgap polymer donor containing an alkylthiophenyl-substituted benzodithiophene moiety. *ChemPhysChem* **2019**, *20*, 2668–2673.
31 Guo, H.; Huang, B.; Zhang, L.; Chen, L.; Xie, Q.; Liao, Z.; Huang, S.; Chen, Y. Double acceptor block-containing copolymers with deep HOMO levels for organic solar cells: adjusting carboxylate substituent position for planarity. *ACS Appl. Mater. Interfaces* **2019**, *11*, 15853–15860.
32 Cho, H. W.; An, N. G.; Park, S. Y.; Shin, Y. S.; Lee, W.; Kim, J. Y.; Song, S. Thermally durable nonfullerene acceptor with nonplanar conjugated backbone for high-performance organic solar cells. *Adv. Energy Mater.* **2020**, *10*, 1903585.
33 Chao, P.; Chen, H.; Zhu, Y.; Lai, H.; Mo, D.; Zheng, N.; Chang, X.; Meng, H.; He, F. A benzo[1,2-b:4,5-*c*']dithiophene-4,8-dione-based polymer donor achieving an efficiency over 16. *Adv. Mater.* **2020**, *32*, e1907059.
34 Zeng, A.; Ma, X.; Pan, M.; Chen, Y.; Ma, R.; Zhao, H.; Zhang, J.; Kim, H. K.; Shang, A.; Luo, S.; Angunawela, I. C.; Chang, Y.; Qi, Z.; Sun, H.; Lai, J. Y. L.; Ade, H.; Ma, W.; Zhang, F.; Yan, H. A chlorinated donor polymer achieving high-performance organic solar cells with a wide range of polymer molecular weight. *Adv. Funct. Mater.* **2021**, *31*, 2102413.
35 Fan, Q.; Zhu, Q.; Xu, Z.; Su, W.; Chen, J.; Wu, J.; Guo, X.; Ma, W.; Zhang, M.; Li, Y. Chlorine substituted 2D-conjugated polymer for high-performance polymer solar cells with 13.1% efficiency via toluene processing. *Nano Energy* **2018**, *48*, 413–420.
36 Wu, J.; Guo, X.; Xiong, M.; Xia, X.; Li, Q.; Fang, J.; Yan, X.; Liu, Q.; Lu, X.; Wang, E.; Yu, D.; Zhang, M. Modulating the nanoscale morphology on carboxylate-pyrazine containing terpolymer toward 17.8% efficiency organic solar cells with enhanced thermal stability. *Chem. Eng. J.* **2022**, *446*, 137424.
37 Qiu, J.; Liu, M.; Wang, Y.; Xia, X.; Liu, Q.; Guo, X.; Lu, X.; Zhang, M. Linear regulating of polymer acceptor aggregation with short alkyl chain units enhances all-polymer solar cells' efficiency. *Macromol. Rapid Commun.* **2022**, *44*, 2200753.
38 Wu, J.; Li, G.; Fang, J.; Guo, X.; Zhu, L.; Guo, B.; Wang, Y.; Zhang, G.; Arunagiri, L.; Liu, F.; Yan, H.; Zhang, M.; Li, Y. Random terpolymer based on thiophene-thiazolothiazole unit enabling efficient non-fullerene organic solar cells. *Nat. Commun.* **2020**, *11*, 4612.
39 Mei, J.; Kim, D. H.; Ayzner, A. L.; Toney, M. F.; Bao, Z. Siloxane-terminated solubilizing side chains: bringing conjugated polymer backbones closer and boosting hole mobilities in thin-film transistors. *J. Am. Chem. Soc.* **2011**, *133*, 20130–20133.
40 Wang, Q.; Hu, Z.; Wu, Z.; Lin, Y.; Zhang, L.; Liu, L.; Ma, Y.; Cao, Y.; Chen, J. Introduction of siloxane-terminated side chains into semiconducting polymers to tune phase separation with nonfullerene acceptor for polymer solar cells. *ACS Appl. Mater. Interfaces* **2020**, *12*, 4659–4672.
41 Feng, S.; Liu, C.; Xu, X.; Liu, X.; Zhang, L.; Nian, Y.; Cao, Y.; Chen, J. Siloxane-terminated side chain engineering of acceptor polymers leading to over 7% power conversion efficiencies in all-polymer solar cells. *ACS Macro Lett.* **2017**, *6*, 1310–1314.
42 Yin, Z.; Guo, X.; Wang, Y.; Zhu, L.; Chen, Y.; Fan, Q.; Wang, J.; Su, W.; Liu, F.; Zhang, M.; Li, Y. Siloxane-functional small molecule acceptor for high-performance organic solar cells with 16.6% efficiency. *Chem. Eng. J.* **2022**, *442*, 136018.
43 Jiang, H.; Pan, F.; Zhang, L.; Zhou, X.; Wang, Z.; Nian, Y.; Liu, C.; Tang, W.; Ma, Q.; Ni, Z.; Chen, M.; Ma, W.; Cao, Y.; Chen, J. Impact of the siloxane-terminated side chain on photovoltaic performances of the dithienylbenzodithiophene-difluorobenzotriazole-based wide band gap polymer donor in non-fullerene polymer solar cells. *ACS Appl. Mater. Interfaces* **2019**, *11*, 29094–29104.
44 Fan, B.; Zhong, W.; Ying, L.; Zhang, D.; Li, M.; Lin, Y.; Xia, R.; Liu, F.; Yip, H. L.; Li, N.; Ma, Y.; Brabec, C. J.; Huang, F.; Cao, Y. Surpassing the 10% efficiency milestone for 1-cm^2 all-polymer solar cells. *Nat. Commun.* **2019**, *10*, 4100.
45 Fan, B.; Zhu, P.; Xin, J.; Li, N.; Ying, L.; Zhong, W.; Li, Z.; Ma, W.; Huang, F.; Cao, Y. High-performance thick-film all-polymer solar cells created *via* ternary blending of a novel wide-bandgap electron-donating copolymer. *Adv. Energy Mater.* **2018**, *8*, 1703085.
46 Zhao, F.; Yuan, Y.; Ding, Y.; Wang, Y.; Wang, X.; Zhang, G.; Gu, X.; Qiu, L. Taming charge transport and mechanical properties of conjugated polymers with linear siloxane side chains. *Macromolecules* **2021**, *54*, 5440–5450.
47 Jing, J.; Dou, Y.; Chen, S.; Zhang, K.; Huang, F. Solution sequential deposited organic photovoltaics: from morphology control to large-area modules. *eScience* **2023**. DOI: 10.1016/j.esci.2023.100142.
48 Chen, X.; Liu, B.; Zou, Y.; Xiao, L.; Guo, X.; He, Y.; Li, Y. A new benzo[1,2-*b*:4,5-*b*']difuran-based copolymer for efficient polymer solar cells. *J. Mater. Chem.* **2012**, *22*, 17724–17731.
49 Kyaw, A. K. K.; Wang, D. H.; Gupta, V.; Leong, W. L.; Ke, L.; Bazan, G. C.; Heeger, A. J. Intensity dependence of current–voltage characteristics and recombination in high-efficiency solution-processed small-molecule solar cells. *ACS Nano* **2013**, *7*, 4569–4577.
50 Riedel, I.; Parisi, J.; Dyakonov, V.; Lutsen, L.; Vanderzande, D.; Hummelen, J. C. Effect of temperature and illumination on the electrical characteristics of polymer-fullerene bulk-heterojunction solar cells. *Adv. Funct. Mater.* **2004**, *14*, 38–44.
51 Gao, W.; Liu, T.; Zhong, C.; Zhang, G.; Zhang, Y.; Ming, R.; Zhang, L.; Xin, J.; Wu, K.; Guo, Y.; Ma, W.; Yan, H.; Liu, Y.; Yang, C. Asymmetrical small molecule acceptor enabling nonfullerene polymer solar cell with fill factor approaching 79%. *ACS Energy Lett.* **2018**, *3*, 1760–1768.
52 Liao, X.; Xie, Q.; Guo, Y.; He, Q.; Chen, Z.; Yu, N.; Zhu, P.; Cui, Y.; Ma, Z.; Xu, X.; Zhu, H.; Chen, Y. Inhibiting excessive molecular aggregation to achieve highly efficient and stabilized organic solar cells by introducing a star-shaped nitrogen heterocyclic-ring acceptor. *Energy Environ. Sci.* **2022**, *15*, 384–394.
53 Xu, G.; Rao, H.; Liao, X.; Zhang, Y.; Wang, Y.; Xing, Z.; Hu, T.; Tan, L.; Chen, L.; Chen, Y. Reducing energy loss and morphology optimization Manipulated by molecular geometry engineering for hetero-junction organic solar cells. *Chin. J. Chem.* **2020**, *38*, 1553–1559.
54 Liao, X.; He, Q.; Zhou, G.; Xia, X.; Zhu, P.; Xing, Z.; Zhu, H.; Yao, Z.; Lu, X.; Chen, Y. Regulating favorable morphology evolution by a simple liquid-crystalline small molecule enables organic solar cells with over 17% efficiency and a remarkable J_{sc} of 26.56 mA/cm^2. *Chem. Mater.* **2021**, *33*, 430–440.